行政院國家科學委員會專題研究計畫成果報告

多環及多管層流擴散火焰之理論分析和實驗研究

Theoretical and Experimental Investigation of Confined Laminar Diffusion Flames in a Multi-Port Burner

計畫編號：NSC 92-2212-E-168-006
執行時間：92 年 08 月 1 日至 93 年 07 月 31 日
計畫主持人：侯順雄教授 崑山科技大學機械系
共同主持人：林大惠教授 國立成功大學機械系

Abstract

The influence of stream concentrations and velocities on the flame structure in a multiple-port burner is theoretically and experimentally studied in this work. A general solution of normal and inverse diffusion flame configurations in a multiple-port burner is obtained with the inclusion of the effects of axial diffusion and unequal stream velocities. The theoretical results show that not only the flame height but also the flame structure is affected by the Peclet number. In the theoretical analysis, the temperature and velocity of stream are two important parameters. Flame configurations can be predicted well by including temperature effect in calculating the Peclet number. For relatively weak (or strong) flame intensity, the prediction of flame configurations agrees well with the experimental results if a lower (or higher) temperature is used. In the experiment, different flame configurations are observed and discussed for various stream velocities and concentrations. The transition of inverse diffusion flame from a single-cone-shaped flame to a double-cone-shaped flame to an envelop flame occurs when the inner stream velocity is adjusted for fixed middle and outer stream velocities. It is of interest to note that under the same operating conditions the flame has history-dependent configuration decided by increasing or decreasing inner stream velocity.

Keywords：Diffusion flame; Multiple-Port burner; Flame transition; Flame configuration

中文摘要

擴散火焰因不需考慮回火的問題，因此在實際工業應用系統是比較安全的。但因擴散火焰之燃料與氧化物是以化學計量比燃燒(stoichiometric burning)，且燃燒氣體在高溫區的遲滯時間較長因而通常會導致較嚴重的污染排放，特別是氮氧化物(NOx)和碳顆粒(soot)。兩環同軸噴流燃燒器中的標準擴散火焰為燃料由中心管噴出，空氣由外環供給。而反置擴散火焰則為空氣由中心管噴出，燃料由外環供給。雖然反置擴散火焰的概念已廣泛應用於諸多重要的氣體燃燒器，但有關反置擴散火焰的文獻卻仍十分匱乏，且大多侷限於兩環同軸反置擴散火焰。有別於以往的文獻，本計畫所提出之中心管噴空氣、第二環噴燃料、第三環噴空氣的三環同軸反置擴散火焰不但能有效降低 NOx 排放和抑制碳顆粒形成，更可用來模擬分段燃燒技術。此外，雖然火焰形狀為層流擴散火焰非常重要的特性，且相當多的理論分析及實驗量測均多所著墨。但理論分析的文獻大多僅侷限於噴流型態擴散火焰

(jet-like diffusion flame)或者典型 Burke-Schumann 擴散火焰, 對於多環同軸標準及反置擴散火焰或多管矩形標準及反置擴散火焰的火焰面預測則尚付之闕如。為了更進一步深入了解多環同軸反置擴散火焰的燃燒特性，並釐清分段燃燒技術的主宰機制，本計畫將以理論分析預測多環同軸和多管矩形具侷限邊界擴散火焰之火焰形狀及高度，探討噴流出口速度、噴流出口幾何尺寸、噴流出口燃料與氧化物濃度、優先擴散(preferential diffusion)及 Pe 數(Peclet number)對火焰形態及其結構之影響。同時將以三環同軸擴散火焰燃燒器之實驗設備探討各噴流管之管徑尺寸大小、噴流出口速度、燃料與氧化物出口濃度、侷限邊界等參數變化對標準和反置擴散火焰的火焰型態和穩定性的影響。理論解並將與實驗結果進行驗證。本計畫之研究成果，在學術探討方面可促進吾人對多環同軸或多管矩形擴散火焰的了解與認識，在實際應用方面可作為工業用爐之燃燒室與燃燒器噴嘴設計之重要參考依據，藉以尋求高效率、省能源、低污染、以及易製造與操作之終極目標。

關鍵詞：Burke-Schumann 擴散火焰，反置擴散火焰，多環及多管燃燒器

1. Introduction

The classical Burke-Schumann diffusion flame has been widely adopted as a model problem for coflowing laminar combustion because of its geometrical and theoretical simplicity (Burke and Schumann, 1928). In the original study, only the diffusion equations were solved, which led to the solution for the flame configuration. However, their formulation has limitations due to several fundamental assumptions. For instance, the effects of the transverse convection and streamwise diffusion are neglected. It is apparent that the neglect of streamwise diffusion limits the applicability and accuracy of the formulation for large Peclet number (Pe) flows.

In Chung and Law's study (1984), the classical Burke-Schumann formulation has been extended to include the effects of both streamwise and preferential diffusion on the flame temperature and characteristics. They found that depending on the effective Lewis number of the fuel and oxidizer, the flame temperature may vary either monotonically or non-monotonically along the flame sheet; and that while for high Peclet number flows the flame height scales with Peclet number, for low Peclet number flows the flame height becomes independent of Peclet number.

Im et al. (1990) have used the same model to investigate the effects of flame curvature on diffusion flame extinction at the opening of Burke-Schumann flame tip. They have successfully demonstrated both theoretically and experimentally that compressive flame curvature tends to promote complete reaction and thereby retard extinction.

The typical research method for Burke-Schumann diffusion flame is to use concentric cylindrical tubes or two-dimensional slot burners in the published works. Chao and Axelbaum (2000) have used the Burke-Schumann methodology to solve the flame structure and flame temperature distribution for three coaxial flows with application to flame synthesis.

Much attention has been paid to the flow-field effects on the flames established in a confined coaxial flow (Barr, 1952; Mitohell and Sarofim, 1980; Wu and Essenhigh, 1984; Gordonet al., 1994; Kaplan and Kailasanath, 2001). However, those studies only focused on coaxial flows with equal fuel and air velocities; there is still a lack of studies on the

characteristics of diffusion flames established in multiple-port coaxial burners, especially for unequal fuel and oxidizer velocities.

Multiple-port burners are widely used to get an extensive and uniform heating surface in common industrial furnaces or domestic stoves. Jet arrays or coaxial jet are two groups of multiple-port burner (Viskanta, 1993). For example, a domestic gas stove is an arrays burner, while a staged-air combustion burner in a boiler is a coaxial jet burner. In engineering applications, one often encounters geometrical arrangements where the burner may be coaxially confined (Viskanta, 1993). The objective of this work is to theoretically predict the flame configurations and to experimentally study the combustion characteristics of confined multiple-port coaxial burners. In the theoretical study we analyze the normal and inverse multiple-port diffusion flames by including: (1) both streamwise (axial) and transverse (radial) diffusion effects, (2) the variations of stream concentration, and (3) both equal or unequal stream (fuel and oxidizer) velocities. The general solutions of the confined multiple-port coaxial normal or inverse diffusion flames are obtained.

In order to reduce soot formation or NOx emission, the inverse diffusion flames are widely used in industrial burners (Partridge Jr and Laurendeau, 1995). Therefore, experimentally, a tri-coaxial burner, in which an inverse diffusion flame can be established, is employed to investigate the flame structure affected by varying the velocities and compositions of the fuel and oxidizer. The results would greatly help us to understand the flame structure and flame height of diffusion flames generated in a multi-port coaxial burner.

2. Formulation

2.1 Basic assumptions

The assumptions in this theoretical study are made as follows:

1. At port exit, the velocities of fuel and oxidizer stream are constant and uniform across their respective tubes.
2. The mass flux in the z-direction is constant for each port exit, that is, $\rho u = \text{constant}$.
3. The fuel and oxidizer reaction for the diffusion flame is one-step overall.
4. The physical properties (e.g. diffusivity, specific heat and thermal conductivity) are constant in the system.
5. The momentum transfer and shearing force are neglected under unequal stream velocity conditions.
6. Unity Lewis number is also assumed in this analysis (Chung and Law, 1984).

2.2 Governing equations

The problem to be analyzed is shown schematically on the left side of Fig. 1, which is a modified version of classical Burke-Schumann flame in a multiple-port coaxial burner for the flame sheet solution. The major improvement in our formulation is the inclusion of the effects of axial diffusion and unequal stream (fuel and oxidizer) velocities, which are neglected in the

conventional Burke-Schumann analysis but are essential for the prediction of flame structure. An axisymmetric flow configuration is adopted in the formulation, with r and z being the radial and axial coordinates, respectively.

Following Williams (1985), the non-dimensional conservation equations for coupling function, $\gamma_{F,O} = \tilde{Y}_F - \tilde{Y}_O$ and $\gamma_{T,j} = \tilde{Y}_j + \tilde{T}$, are, respectively, given by

$$Pe\frac{\partial(\gamma_{F,O})}{\partial\eta} - \left[\frac{1}{\xi}\frac{\partial}{\partial\xi}\left(\xi\frac{\partial(\gamma_{F,O})}{\partial\xi}\right) + \frac{\partial^2(\gamma_{F,O})}{\partial\eta^2}\right] = 0 \tag{1}$$

$$Pe\frac{\partial(\gamma_{T,j})}{\partial\eta} - \left[\frac{1}{\xi}\frac{\partial}{\partial\xi}\left(\xi\frac{\partial(\gamma_{T,j})}{\partial\xi}\right) + \frac{\partial^2(\gamma_{T,j})}{\partial\eta^2}\right] = 0, \text{ where j=F or O} \tag{2}$$

These equations are subjected to the multi-port boundary conditions:

$\eta > 0,\ \xi = 0:\ \partial(\ )/\partial\xi = 0$ (symmetry) (3)

$\eta > 0,\ \xi = 1:\ \partial(\ )/\partial\xi = 0$ (adiabatic, impermeable wall) (4)

$\eta = 0,\ c_{i-1} \le \xi < c_i:\ \tilde{Y}_j = \tilde{Y}_{i,j} \times d_i,\ \tilde{T} = \tilde{T}_0$ (5)

$\eta \to \infty,\ 0 \le \xi \le 1$: boundedness (6)

where η and ξ are, respectively, the axial and radial coordinates normalized by the outermost radius (r_s). c_i is the ratio of the radius of the i-th ring (r_i) to the outermost radius (r_s). d_i is the ratio of the i-th stream velocity to the reference stream velocity ($d_i = u_i / u_{ref}$). The Pelet number is defined as $Pe \equiv \rho u_{ref} r_s / (\lambda C_P)$, where ρ, λ and C_P are each a function of stream temperature at the burner exit. Furthermore, u_{ref} is the characteristic axial velocity. The rest of the symbols are conventional and can be found in Chung and Law's study (1984).

Using the method of separation of variables, Eqs. (1) and (2) subjected to the boundary conditions, namely Eqs. (3)-(6), can be solved. The general solutions are obtained as follows:

$$\gamma_{T,F} = \tilde{T}_0 + A_{0,M} + \sum_{n=1}^{\infty} A_{n,M} \frac{2}{\phi_n J_0^2(\phi_n)} J_0(\phi_n \xi) \exp\left(\frac{Pe - \sqrt{Pe^2 + 4\phi_n^2}}{2}\eta\right) \tag{7}$$

$$\gamma_{T,O} = \tilde{T}_0 + B_{0,M} + \sum_{n=1}^{\infty} B_{n,M} \frac{2}{\phi_n J_0^2(\phi_n)} J_0(\phi_n \xi) \exp\left(\frac{Pe - \sqrt{Pe^2 + 4\phi_n^2}}{2}\eta\right) \tag{8}$$

$$\gamma_{F,O} = (A_{0,M} - B_{0,M}) + \sum_{n=1}^{\infty} (A_{n,M} - B_{n,M}) \frac{2}{\phi_n J_0^2(\phi_n)} J_0(\phi_n \xi) \exp\left(\frac{Pe - \sqrt{Pe^2 + 4\phi_n^2}}{2}\eta\right) \tag{9}$$

where

$$A_{o,M} = \sum_{l=1}^{M'} (\tilde{Y}_{2l-1,j} \times d_{2l-1})[(-1)^{2l} c_{2l-1}^2 + (-1)^{2l+1} c_{2l-2}^2] \quad (10)$$

$$A_{n,M} = \sum_{l=1}^{M'} (\tilde{Y}_{2l-1,j} \times d_{2l-1})[(-1)^{2l} c_{2l-1} J_1(c_{2l-1}\phi_n) + (-1)^{2l+1} c_{2l-2} J_1(c_{2l-2}\phi_n) \quad (11)$$

$$B_{o,M} = \sum_{l=1}^{M'} (\tilde{Y}_{2l,j} \times d_{2l})[(-1)^{2l} c_{2l}^2 + (-1)^{2l+1} c_{2l-1}^2] \quad (12)$$

$$B_{n,M} = \sum_{l=1}^{M'} (\tilde{Y}_{2l,j} \times d_{2l})[(-1)^{2l} c_{2l} J_1(c_{2l}\phi_n) + (-1)^{2l+1} c_{2l-1} J_1(c_{2l-1}\phi_n) \quad (13)$$

($M' = \frac{M}{2}$ as M (the number of rings) is even, $M' = \frac{M-1}{2}$ as M is odd)

and J_i is the Bessel function of the first kind of order i and ϕ_n is the nth positive root of $J_1(\phi) = 0$.

The problem is now reduced to the solutions of the coupling functions $\gamma_{F,O} = \tilde{Y}_F - \tilde{Y}_O$ and $\gamma_{T,j} = \tilde{Y}_j + \tilde{T}$.

2.3 Flame sheet solution

On the flame sheet, the flame temperature can be obtained from Eqs. (7) ~ (9) by setting $\gamma_{F,O} = 0$ and $\gamma_{T,F} = \gamma_{T,O} = \tilde{T}_f$ ($\tilde{Y}_j = 0$). Furthermore, the flame location $(\xi_f,\ \eta_f)$ is defined by the following equation

$$A_{0,M} - B_{0,M} = \sum_{n=1}^{\infty} (B_{n,M} - A_{n,M}) \frac{2}{\phi_n J_0^2(\phi_n)} J_0(\phi_n \xi_f) \exp\left(\frac{Pe - \sqrt{Pe^2 + 4\phi_n^2}}{2} \eta_f\right) \quad (14)$$

The general solution derived above is suitable for normal or inverse diffusion flames in a multiple-port burner with various number of concentric tubes.

3. Experimental setup

The combustion system, schematically depicted on the left side of Fig. 1, consists of three concentric tubes of radii r_1 = 13 mm, r_2 = 28 mm and r_s = 60 mm through which the oxidizer (mixture of oxygen and nitrogen), methane, and oxidizer (mixture of oxygen and nitrogen) flow out, respectively. That is, the concentric-tube burner consists of a central jet surrounded by two annular regions. Inverse diffusion flames, which are extensively used in industrial burners, can be established by introducing an annular fuel jet sandwiched between an axisymmmetric oxidizer jet (on the inside) and an coflowing annular jets oxidizer (on the outside).

For the outermost tube ($r = r_s$), we set up a cylindrical quartz shield as the confining wall. Several layers of honeycombs and meshed screens are installed inside the coaxial tubes in order to produce a uniform velocity distribution at the exit plane of the tubes. Methane, nitrogen and

oxygen are separately controlled by conventional rotameters and pressure gauges.

In the experiment, the compositions of the inner and outer oxidizer streams and the stream (fuel or oxidizer) velocities can be adjusted. The measurement of flame structure and flame height will be compared with the results of the theoretical model.

4. Results and discussion

In order to compare experimental data with theoretical results, we simplify the general solutions of the theoretical model by setting M=3 and using u_2 as the reference stream velocity. Hence, Eqs. (9) ~ (14) become, respectively,

$$A_{0,3} - B_{0,3} = \sum_{n=1}^{\infty} (B_{n,3} - A_{n,3}) \frac{2}{\phi_n J_0^2(\phi_n)} J_0(\phi_n \xi) \exp\left(\frac{Pe - \sqrt{Pe^2 + 4\phi_n^2}}{2} \eta\right) \tag{15}$$

$$A_{o,3} = [\tilde{Y}_{1,O} \times (u_1/u_2)] c_1^2 + [\tilde{Y}_{3,O} \times (u_3/u_2)](1 - c_2^2) \tag{16}$$

$$A_{n,3} = [\tilde{Y}_{1,O} \times (u_1/u_2)] c_1 J_1(c_1\phi_n) - [\tilde{Y}_{3,O} \times (u_3/u_2)] c_2 J_1(c_2\phi_n) \tag{17}$$

$$B_{o,3} = \tilde{Y}_{2,F} \times (c_2^2 - c_1^2) \tag{18}$$

$$B_{n,3} = \tilde{Y}_{2,F} \times [c_2 J_1(c_2\phi_n) - c_1 J_1(c_1\phi_n)] \tag{19}$$

The effect of the Peclet number (Pe) on the flame structure for equal stream velocities ($u_3/u_2 = 1, u_1/u_2 = 1$) and a fixed concentration combination, i.e.[Ω_{1,O_2}, Ω_{2,CH_4}, Ω_{3,O_2}] = [100, 64, 100], is shown on the right side of Fig. 1. Note that Ω is the volumetric percentage of methane or oxygen, and subscripts 1, 2 and 3 represent inner, middle and outer stream, respectively. The radius of inner and middle tube, c_1 and c_2, of the tri-coaxial burner adopted corresponds to $\xi = 0.25$ and 0.47, respectively. The theoretical results indicate that for large Peclet number (Pe=10 and 50), the double-flame structure comprises a conical inner diffusion flame (IDF) and a conical outer diffusion flame (ODF). The flame height of ODF lengthens with enlarging Pe. At Pe=5, the central part of ODF is slightly concave and the distance between the IDF and ODF decreases. Further decrease in Pe leads to the envelope flame at Pe=1. The establishment of the envelope flame implies that the flame sheet of IDF connects with that of ODF. Note that not only flame height but also flame structure are significantly affected by the Peclet number. This significant characteristic, i.e. the flame structure can be affected by the Peclet number, differs from classical Burke-Schumann diffusion flame. In general, the Peclet number is a function of the physical properties and velocity of stream. However, physical properties depend on stream temperature, which can be raised by preheating. In this study, for the same stream velocity, at low temperatures, the Peclet number is about 200; while at very high temperatures, e.g. 2000 K, the Peclet number reduces to Pe=4. It is clear that the magnitude of Pe is

considerably affected by the temperature.

4.1 Equal fuel and oxidizer velocities

Figure 2 depicts the direct photographs of the flame appearance influenced by inner and outer oxidizer concentrations for an annular pure fuel jet at equal fuel and oxidizer velocity $(V_1, V_2, V_3) = (4,\ 4,\ 4)$ in cm/sec. For the same column of photographs, the inner oxidizer and middle fuel stream concentrations are fixed but the outer stream concentration varies from 21% to 80%. For the same row, the middle fuel and outer oxidizer stream concentrations are constant but the inner oxidizer stream concentration varies from 40% to 100%. In the first row, the outer stream is air. It is found that the tip of the ODF is open and the IDF is a conical shape diffusion flame. Increasing the inner oxidizer concentration (Ω_{1,O_2}) does not change the flame structure, as shown in the first row. Moreover, the flame height is independent of the inner oxidizer concentration. This is because the ODF fluctuates greatly under this operating condition.

In the second row, the flame structure becomes a double-cone-shaped flame (both IDF and ODF are conical). The flame height of ODF (or IDF) decreases with increasing (or decreasing) Ω_{1,O_2}. In the third row, the flame structure shows the same trend as that in the second row except that the IDF and ODF slant to the middle fuel stream and generate an envelop flame at $[\Omega_{1,O_2},\ \Omega_{2,CH_4},\ \Omega_{3,O_2}] = [100,\ 100,\ 60]$. This indicates that the flame height of IDF is high enough to connect with ODF and then an envelop flame is established. The flame structures in the fourth row are the same as those in the third row. However, the flame height is shorter.

In the experiment, the inner and outer stream concentrations (Ω_{1,O_2} and Ω_{3,O_2}) play an important role on the flame configuration. For example, as shown in the third column, three kinds of flame configuration appear by varying Ω_{3,O_2} from 21% to 60%. But the envelope flame does not appear in the first column. It indicates that the envelop flame can only be established when both Ω_{1,O_2} and Ω_{3,O_2} are large enough. The flame intensity is enhanced by increasing the concentration of oxygen, Ω_{1,O_2} or Ω_{3,O_2}. The flame color in the first row is yellow but is brightly white in the fourth row.

Figure 3 shows the flame structure predicted by the theoretical model. In the theoretical derivation, the Peclet number is a function of temperature and stream velocity. In order to relieve the effect of velocity, the stream velocity is fixed at 4 cm/sec. Four values of temperature (300 K, 500 K, 1000 K and 2000 K) are used to calculate the Peclet number (corresponding to Pe=105, 40, 12 and 4, respectively). The increase of temperature results in the decrease of the Peclet number. It is seen that the flame height increases with increasing Peclet number (decreasing temperature), which is consistent with earlier studies by Burke and Schumann (1928) and Chung and Law (1984).

When the ODF slants to the outer stream and the IDF is a conical flame, the flame height is relatively high and the burning intensity is not strong (as shown in Fig. 2), so that the temperature

is low. In our theoretical prediction, the flame configuration predicted by using a high Pe (based on 300 K) agrees well with the experimental results. At lower flame height, especially for high Ω_{3,O_2}, the flame structure can be predicted well by using 2000 K to calculate the Peclet number. With increasing Ω_{1,O_2} and Ω_{3,O_2}, the flame structure comprises a conical IDF and a conical ODF. The trend of variations of flame structure with Ω_{1,O_2} and Ω_{3,O_2} can be predicted well by using a suitable Pe based on the temperature.

4.2 Unequal fuel and oxidizer velocities

The effect of unequal stream velocity for the fuel and the oxidizer on flame structure is theoretically and experimentally studied in this section.

4.2.1 Flame structure

Figure 4 shows that there are eight kinds of flame structure for various stream velocities. In order to get stable flame structure, the middle stream velocity (V_2) varies from 2 cm/sec to 5 cm/sec. The solid line with circles denotes the critical line of IDF ignition and the solid line with triangles designates the critical line where envelop flame is generated. At V_2 = 2 cm/sec, the flame structure changes from single-cone-shaped flame (Type A flame), through double-cone-shaped flame (Type B flame) to envelop shape flame (Type C flame) with increasing inner stream velocity (V_1) from 0 to 40 cm/sec. However, if the inner stream velocity decreases from 40 to 0 cm/sec, the critical line of IDF extinction, indicated by the "Extinction" line, is not the same as that of IDF ignition. The reason can be clearly explained by the classical S-shaped ignition-extinction curve that the ignition state and the extinction state of the same reactants are different, and the extinction Damköhler number is lower than the ignition Damköhler number.

At V_2 =3 cm/sec, Type A, Type B and Type C flames are also observed. Additionally, the tip opening of ODF occurs for $V_2 > V_3$ (namely Type D and Type E flames). At V_2 = 4 cm/sec, for $V_3 \leq 3$ cm/sec, the ODF slants to the outer stream, thus Type F and Type G flames can be generated. For large V_1, both the IDF and ODF are open (Type H flame). The dashed lines represent the critical lines when tip opening of ODF occurs. The dot-dash lines designate the ODF slants to the middle or outer stream. In the experiment, if $V_3 > V_2$, the flame is stable and a conical ODF can be generated. On the contrary, if $V_3 < V_2$, ODF slants to the outer stream and the flame becomes unstable. In other words, the flame structure is strongly influenced by stream velocity.

4.2.2 Flame transition

To gain a better understanding on the flame transition, we vary V_1 but keep V_2 and V_3 constant to observe the variation of flame structure for $[\Omega_{1,O_2}, \Omega_{2,CH_4}, \Omega_{3,O_2}] = [21, 100, 21]$. For V_2=2 cm/sec and V_3=10 cm/sec ($V_2 < V_3$), the results are shown in the upper (or lower) part of Fig. 5 with increasing V_1 from 0 to 20 cm/sec (or decreasing V_1 from 20 to 0 cm/sec). The direct

photograph shows that the condition of ODF slanting to the middle stream and the ignition of IDF are strongly influenced by the inner stream velocity. As V_1 increases from 0 to 8 cm/sec, the IDF can not be generated due to the lack of ignition mechanism (methane from the middle stream and oxygen from the inner stream mix but can not be ignited). At $(V_1, V_2, V_3) = (8, 2, 10)$, the blue weak curved flame front, which is a partially premixed flame, can stabilize at a certain distance above the burner exit but below the outer diffusion flame. The detailed process will be discussed in Fig. 7. The flame color changes from yellow to blue by increasing inner stream velocity (V_1), corresponding to the increases of the amount of inner oxygen. When V_1 exceeds the critical value, the IDF can be ignited and the ODF becomes a yellow diffusion flame again. After the IDF is established, the increase in inner stream velocity rapidly lengthens the flame height of the IDF but shortens the flame height of the ODF. The envelop flame occurs when the inner stream velocity is large enough (V_1>15 cm/sec).

If we reverse the process by decreasing V_1 from 20 to 0 cm/sec, it is seen that the critical point where the envelop flame transforms into the double-cone-shaped flame is slightly different from the critical point where the double-cone-shaped flame transforms into the envelop flame shown on the upper part of Fig. 5; and the extinction point of IDF is not the same as the ignition point. It means that history-dependent configuration exist as the value of V_1 is varied in the range of 1 to 10 cm/sec.

In another special case for V_2=4 cm/sec and V_3=2 cm/sec (V_2>V_3), the direct photographs of increasing V_1 from 0 to 40 cm/sec (or decreasing from 40 to 0 cm/sec) are show in the upper (or lower) part of Fig. 6, respectively. In these conditions, the ODF slants to outer stream, and the IDF is affected by the inner stream velocity. The flame is unstable and the tail of ODF tends to attach to the confining wall. The variations of IDF structure with varying inner stream velocity through different adjusting process have the same trend as in Fig. 5. As V_1 increases from 0 to 10 cm/sec, the IDF can not be developed and the ODF slants to outer stream (defined as Type H flame in Fig. 4). When inner stream velocity exceeds 15 cm/sec, the IDF can be generated (defined as Type G flame in Fig. 4). If we reverse the adjusting process, that is, decreasing the inner stream velocity from 40 to 0 cm/sec, it is found that the extinction point is not the same as the ignition point for IDF. History-dependent configurations also exist for the same flow condition of V_1 in the range from 0 to 15 cm/sec.

It is of interest to note that the flame structure strongly depends on the adjusting process. In the following, we pay our attention on the flame height for V_2=2 cm/sec. In this condition, the ODF slants to the middle stream and the flame is more stable than the condition that the ODF slants to the outer stream. We find that two groups can be sorted out in Fig. 7. The first group occurs for V_3=V_2=2 cm/sec, which is shown by the open circles. The second one appears for V_3>V_2=2 cm/sec, and the flame structure is represented by Type B flame in Fig. 4. The flame height decreases with increasing V_1. Near the critical point of the establishment of IDF, the height increases abruptly and then decreases with increasing V_1. The photographs shown in Fig. 7 reveal that the flame transition from a single conical flame (ODF), through an outer conical ODF with

an inner weak blue flame, and finally to the double-cone-shaped flame (the establishment of stable IDF and ODF). Before IDF is established, there is a blue curved flame sheet at a distance away from the burner exit but below the tip of the ODF at $(V_1, V_2, V_3) = (8, 2, 10)$. Increasing inner stream velocity corresponds to the increase of the amount of oxygen. The burning intensity of the partially premixed flame is enhanced and thus it drops back to the inner tube rim. Hence, at $(V_1, V_2, V_3) = (8.5, 2, 10)$ the partially premixed flame moves toward the burner exit, and then IDF is generated. Furthermore, the characteristic of flame transition for $V_3 > V_2$ is similar to that for $V_3 = V_2$ described above.

4.2.3 Theoretical prediction

The prediction of flame configuration for different stream velocities (by varying V_1 but keeping V_2 and V_3 fixed) at constant stream concentration ($[\Omega_{1,O_2}, \Omega_{2,CH_4}, \Omega_{3,O_2}] = [21, 100, 21]$) is shown in Fig. 8. As discussed in Fig. 3, good prediction can be obtained by considering the dependence of the Peclet number on temperature. In Fig. 8, the lower (or upper) row shows the prediction of flame configurations corresponding to those in Fig. 5 (or Fig. 6). As indicated in the lower row of Fig. 8, when the flame height is high, the flame configurations can be predicted well by using the results of 500 K. However, when the flame height is short, e.g. the envelop flame, good prediction of the flame configurations can be obtained by using 2000 K to calculate the Peclet number.

As the ODF is open and slants to outer stream (corresponding to the photographs shown in Fig. 6), the upper row of Fig. 8 shows that good prediction can be obtained by using the results of 500K. The reason is that the burning intensity is relatively weak, leading to the relatively low temperature. It is concluded that the prediction of flame configurations shows good agreement with the experimental results by selecting a suitable Peclet number depending on the temperature.

5. Conclusions

A theory of normal and inverse diffusion flames in a multiple-port coaxial burner was developed to explore the influences of stream concentration, stream velocity and Peclet number on the flame structure. In the experiment, the concentric-tube burner, which consists of a central jet surrounded by two annular regions, was set up to investigate the combustion characteristics of inverse diffusion flames. Inverse diffusion flames, which are extensively used in industrial burners, can be developed by introducing an annular fuel jet sandwiched between an axisymmmetric oxidizer jet (on the inside) and a coflowing oxidizer (on the outside). The results are generally concluded as follows:

(1) A general solution of normal and inverse diffusion flame configurations in a multi-port burner with the inclusion of the effects of axial diffusion and unequal stream velocities can be obtained. It is found that not only the flame height but also the flame structure is significantly affected by the Peclet number.

(2) In calculating the Peclet number, temperature and velocity of stream are two important parameters. Flame configurations can be predicted well by including the temperature effect in calculating the Peclet number. For relatively weak (or strong) flame intensity, the prediction of flame configurations agrees well with the experimental results by using a lower (or higher) temperature.

(3) In the experiment, different flame configurations are observed by varying stream velocity or concentration. If $V_3 > V_2$, the flame is stable and a conical flame can be generated. On the contrary, if $V_3 < V_2$, the outer diffusion flame slants to the outer stream and the flame become unstable.

(4) The transition from a single-cone-shape flame, to a double-cone-shaped flame, to an envelop flame takes place by adjusting the inner stream velocity. It is interesting to note that under the same operating conditions the flame has history-dependent configurations decided by gradually increasing or decreasing inner stream velocity.

(5) If the inner stream velocity is not large enough, the blue weak curved flame front, which is a partially premixed flame, can stabilize at a certain distance above the burner exit but below the outer diffusion flame at the critical stream velocity $(V_1, V_2, V_3)=(8, 2, 10)$. With increasing inner stream velocity (corresponding to increasing amount of oxygen), the intensified curved flame drops back, then it disappears and is replaced by the yellow inner diffusion flame.

6. 計畫成果自評

(1) 本計畫成果目前已投稿國際著名期刊 Combustion Science and Technology 論文一篇及發表中華民國第十四屆燃燒科技應用研討會一篇，其餘成果亦正準備發表中，成果斐然。

(2) 由於考慮軸向擴散和非等速兩項效應的多環同軸標準及反置擴散火焰之火焰面預測的相關研究尚付之闕如，因此，本計畫具有高度原創性與重要性。本研究計畫內容與原計畫內容完全相符，而且百分之百達成預期目標。

(3) 本計畫提出之理論模式，可用來預測多管或多管噴流擴散火焰之火焰高度及其結構。並已利用實驗驗證其理論模式之正確性。

(4) 本計畫提出之反置擴散火焰概念，可避免傳統噴流擴散燃燒火焰燃燒時會有 NO_X 與 soot 過多之情形發生，直接從燃燒器設計本身著手，利用反置擴散火焰之觀念，用以模擬分段燃燒技術，來達到降低 NO_X 與 soot 的目的。

(5) 本計畫之研究成果，在學術探討方面可促進吾人對反置擴散火焰的了解與認識，在實際應用方面可作為工業爐燃燒器噴嘴設計與燃燒室設計之重要參考依據，藉以尋求高效率、省能源、低污染、以及易製造與操作之終極目標。

Acknowledgements

This work was supported by the National Science Council, Taiwan, ROC, under the contract of NSC 92-2212-E-168-006.

References

Barr, J. (1952). Flames of fuel jets. Proc. Comb. Inst. **4**, 765.

Burke, S.P., and Schumann, T.E.W. (1928). Diffusion flames. *Proc. Combust. Inst.*, **1,** 2.

Chao, B.H., and Axelbaum, R.L. (2000). Tri-axial Burke-Schumann flames withapplications to flame synthesis. *Combust. Sci. Tech.*, **156**, 291.

Chung, S.H., and Law, C.K. (1984). Burke-Schumann flame with streamwise and preferential diffusion. *Combust. Sci. Tech.*, **37**, 21.

Gordon, A.S., Li, S.C., Libby, P.A., and Williams, F.A. (1994). Influence of initial velocity distribution on the height of methane-air nonpremixed flames. *Combust. Sci. Tech.*, **100**, 395.

Im, H.G., Law, C.K., and Axelbaum, R.L. (1990). Opening of the Burke-Schumann flame tip and the effects of curvature on diffusion flame extinction. *Proc. Comb. Inst.* **23,** 551.

Kaplan, C.R., and Kailasanath, K. (2001). Flow-field effects on soot formation in normal and inverse methane-air diffusion flames. *Combust. Flame*, **124**, 275.

Ko, Y. C., Hou, S. S., and Lin, T. H. (2004). Laminar diffusion flames in a multi-port burner. *Combustion Science and Technology*, in revision. (NSC 92-2212-E-168-006)

Mitchell, R.E., Sarofim, A.F., and Clomburg, L.A. (1980). Experimental and numerical investigation of confined laminar diffusion flames. *Combust. Flame*, **37**, 227.

Partridge Jr W.P., and Laurendeau, N.M. (1995). Nitric oxide formation by inverse diffusion flames in staged-air burners. *Fuel*, **74**, 1424.

Viskanta, R. (1993). Heat transfer to impinging isothermal gas and flame jets. *Experimental Thermal and Fluid Science*, **6**, 111.

Williams, F.A., (1985). Combustion Theory, Benjamin-Cummings, Palp Alt.

Wu, K.T., and Essenhigh, R.H., (1984). Mapping and structure of inverse diffusion flames of methane. *Proc. Comb. Inst.*, **20**, 1925.

柯永章, 侯順雄和林大惠(2004), 反置 Burke-Schumann 火焰,中華民國第十四屆燃燒科技應用研討會, 台灣桃園中壢中央大學, 中華民國九十三年三月二十三日。

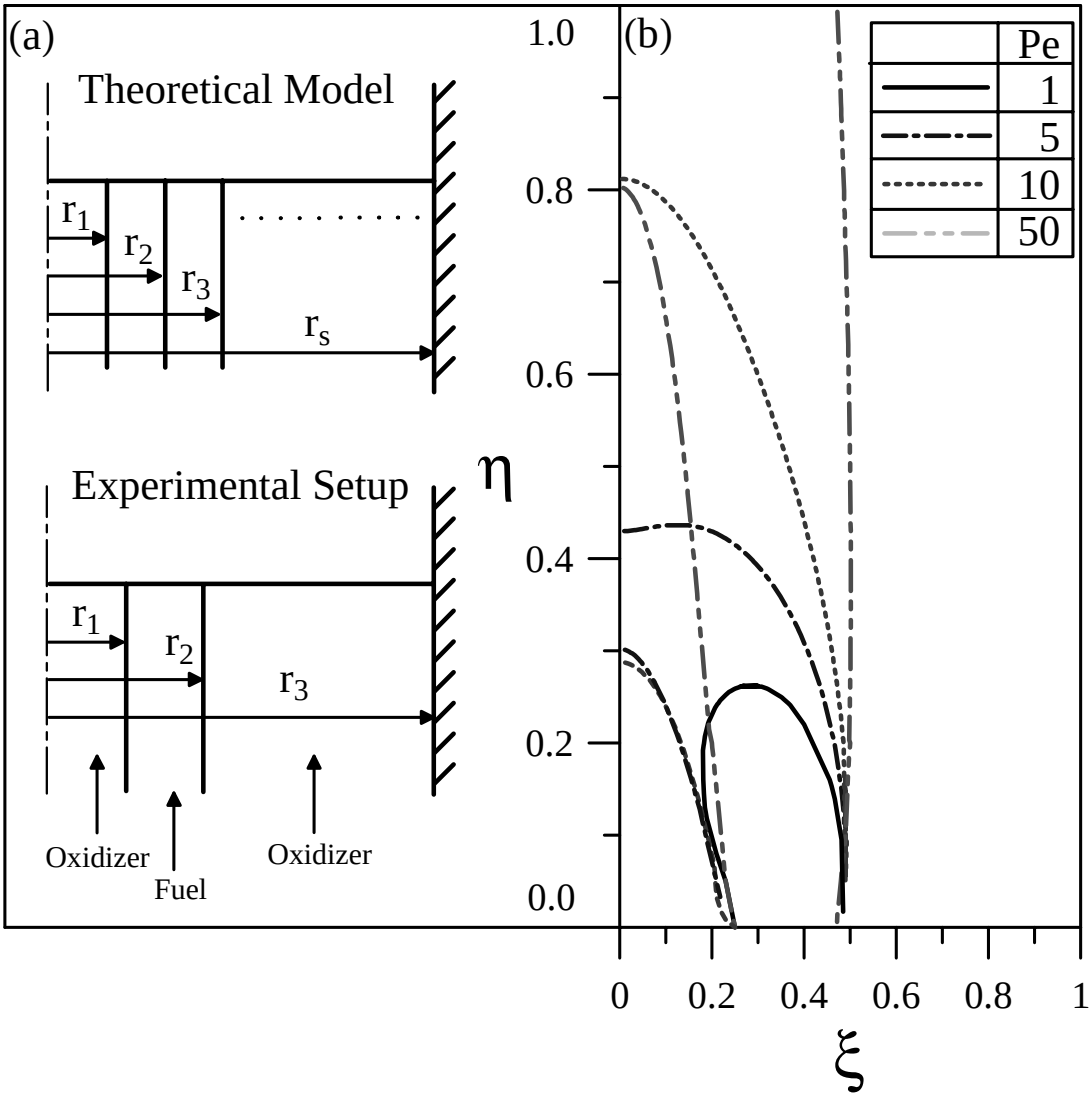

Figure 1 (a) The schematic diagrams of theoretical model and experimental setup. (b) Effect of Peclet number on flame structure and height.

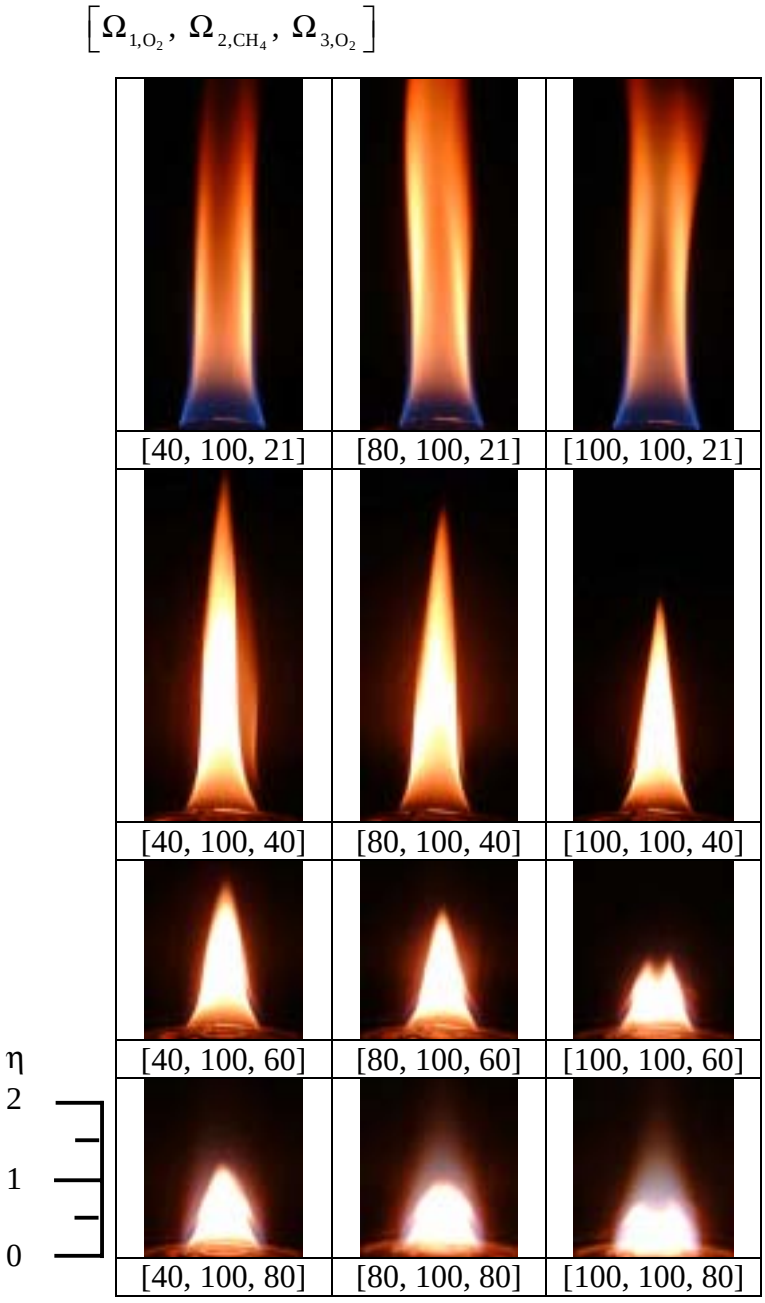

Figure 2 Direct photographs of flame appearances for different stream concentrations at constant stream velocity.

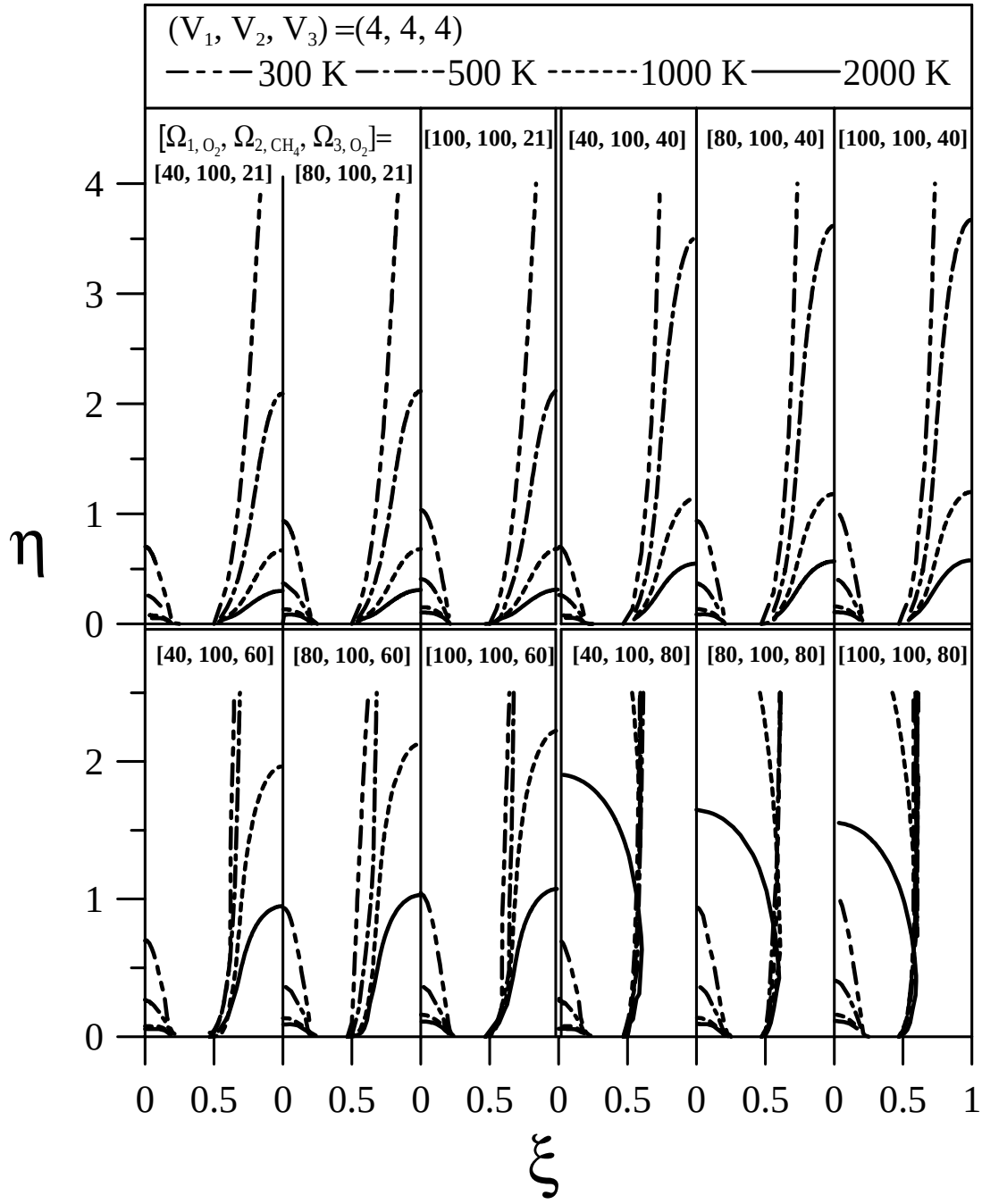

Figure 3 The prediction of flame configuration for different stream concentrations and constant stream velocity $(V_1, V_2, V_3) = (4, 4, 4)$.

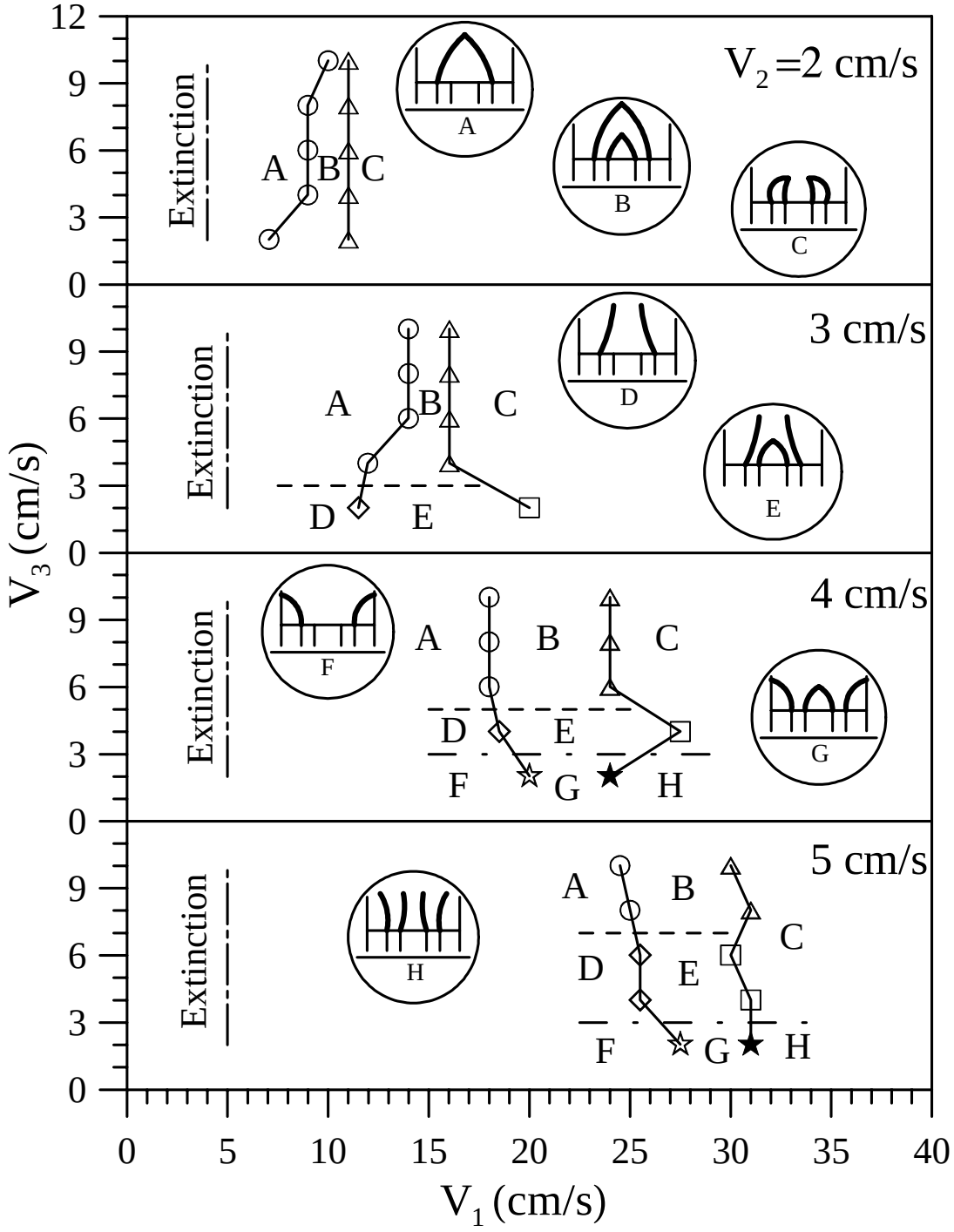

Figure 4 Map of flame configurations of tri-coaxial burner with different stream velocities.

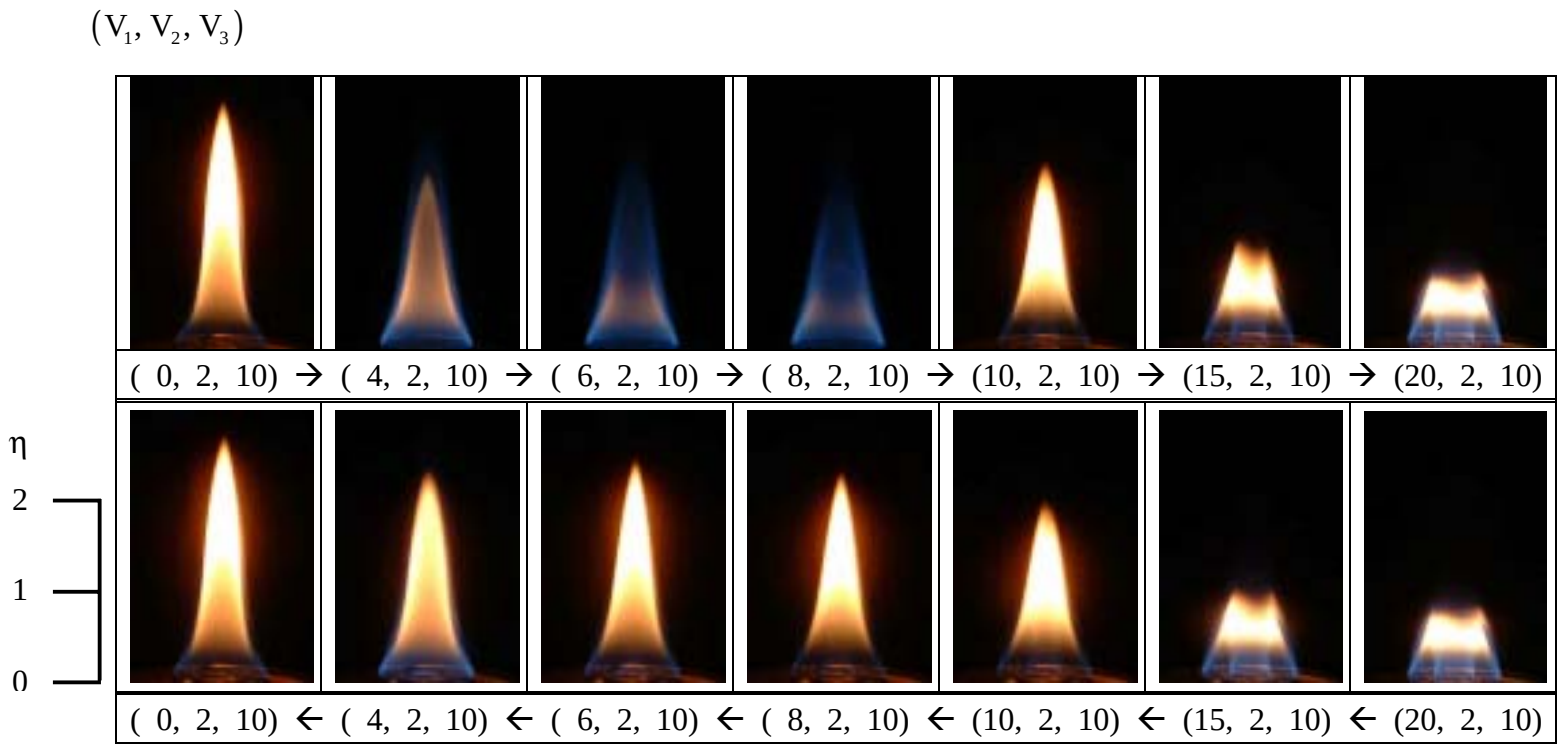

Figure 5 Direct photographs of flame transition at $(V_2, V_3) = (2\ \text{cm/sec},\ 10\text{cm/sec})$ by increasing or decreasing V_1.

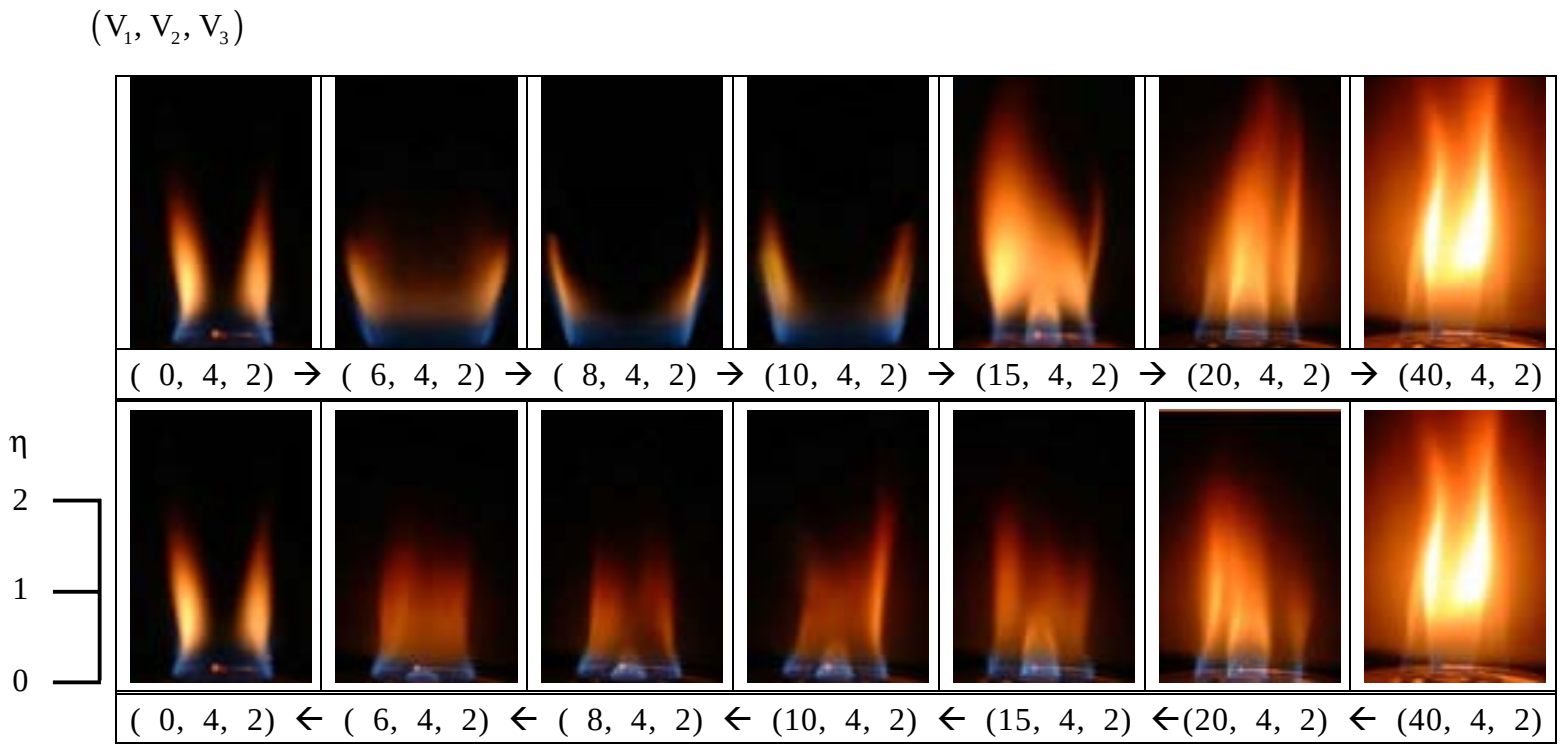

Figure 6 Direct photographs of flame transition at $(V_2, V_3) = (4\ \text{cm/sec},\ 2\text{cm/sec})$ by increasing or decreasing V_1.

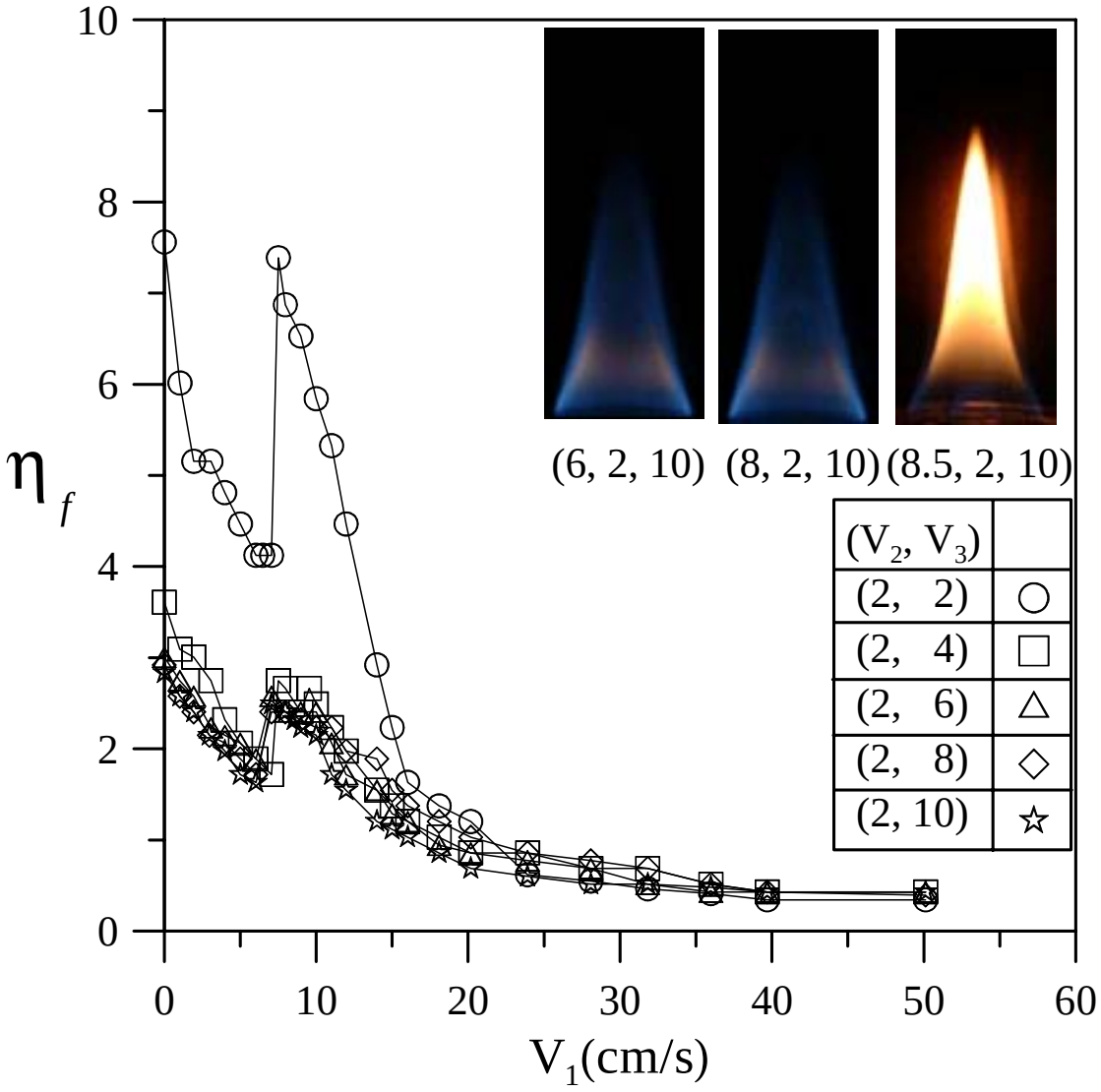

Figure 7 Effect of inner stream velocity (V_1) on flame height.

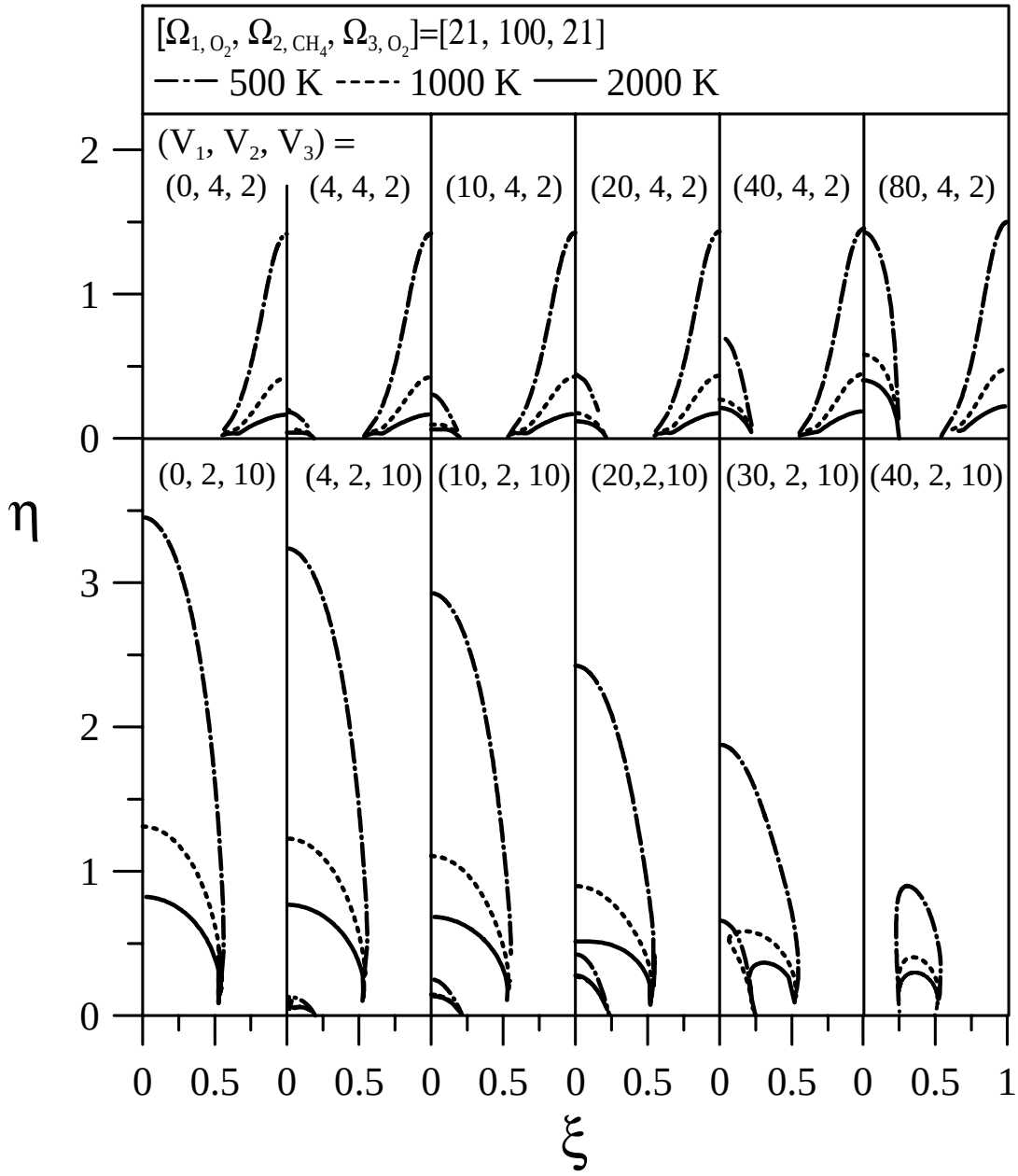

Figure 8 The prediction of flame configuration for different stream velocities at constant stream concentration.